

Interfacial Tensions, Solubilities, and Transport Properties of the H₂/H₂O/NaCl System A Molecular Simulation Study

van Rooijen, W. A.; Habibi, P.; Xu, K.; Dey, P.; Vlugt, T. J.H.; Hajibeygi, H.; Moulτος, O. A.

DOI

[10.1021/acs.jced.2c00707](https://doi.org/10.1021/acs.jced.2c00707)

Publication date

2023

Document Version

Final published version

Published in

Journal of Chemical and Engineering Data

Citation (APA)

van Rooijen, W. A., Habibi, P., Xu, K., Dey, P., Vlugt, T. J. H., Hajibeygi, H., & Moulτος, O. A. (2023). Interfacial Tensions, Solubilities, and Transport Properties of the H₂/H₂O/NaCl System: A Molecular Simulation Study. *Journal of Chemical and Engineering Data*, 69 (2024)(2), 307-319. <https://doi.org/10.1021/acs.jced.2c00707>

Important note

To cite this publication, please use the final published version (if applicable).
Please check the document version above.

Copyright

Other than for strictly personal use, it is not permitted to download, forward or distribute the text or part of it, without the consent of the author(s) and/or copyright holder(s), unless the work is under an open content license such as Creative Commons.

Takedown policy

Please contact us and provide details if you believe this document breaches copyrights.
We will remove access to the work immediately and investigate your claim.

Interfacial Tensions, Solubilities, and Transport Properties of the H₂/H₂O/NaCl System: A Molecular Simulation Study

W. A. van Rooijen,[§] P. Habibi,[§] K. Xu, P. Dey, T. J. H. Vlugt, H. Hajibeygi, and O. A. Moulτος^{*}Cite This: <https://doi.org/10.1021/acs.jced.2c00707>

Read Online

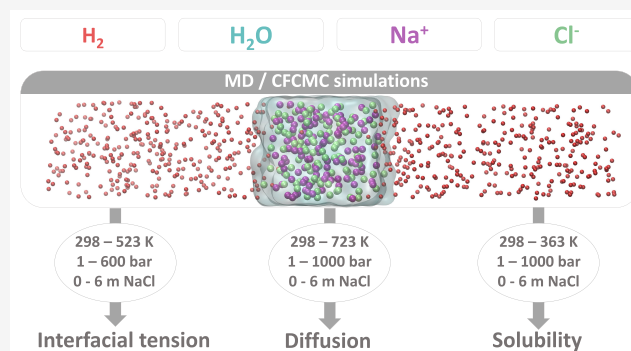
ACCESS |

Metrics & More

Article Recommendations

Supporting Information

ABSTRACT: Data for several key thermodynamic and transport properties needed for technologies using hydrogen (H₂), such as underground H₂ storage and H₂O electrolysis are scarce or completely missing. Force field-based Molecular Dynamics (MD) and Continuous Fractional Component Monte Carlo (CFCMC) simulations are carried out in this work to cover this gap. Extensive new data sets are provided for (a) interfacial tensions of H₂ gas in contact with aqueous NaCl solutions for temperatures of (298 to 523) K, pressures of (1 to 600) bar, and molalities of (0 to 6) mol NaCl/kg H₂O, (b) self-diffusivities of infinitely diluted H₂ in aqueous NaCl solutions for temperatures of (298 to 723) K, pressures of (1 to 1000) bar, and molalities of (0 to 6) mol NaCl/kg H₂O, and (c) solubilities of H₂ in aqueous NaCl solutions for temperatures of (298 to 363) K, pressures of (1 to 1000) bar, and molalities of (0 to 6) mol NaCl/kg H₂O. The force fields used are the TIP4P/2005 for H₂O, the Madrid-2019 and the Madrid-Transport for NaCl, and the Vrabec and Marx for H₂. Excellent agreement between the simulation results and available experimental data is found with average deviations lower than 10%.



1. INTRODUCTION

Due to the vastly growing global energy demand and the resulting climate change, a transition from fossil-fuel based energy production to clean renewable energy production is crucial.^{1,2} As a green energy carrier, hydrogen (H₂) plays a crucial role in this transition because of its high gravimetric energy density and clean combustion products.^{3–5} Important technologies in the H₂ value chain include underground H₂ storage^{6–9} and H₂O electrolysis.^{10,11} To enable the design and optimization of these technologies, accurate knowledge of thermodynamic, interfacial, and transport properties of H₂ is essential.^{9,12–15} More specifically, the diffusivities and solubilities of H₂ in aqueous solutions, and the interfacial tensions of H₂ gas in contact with aqueous electrolyte solutions are crucial properties. The interplay of these properties determines the efficiency of the technologies, and allows for accurate predictions of the processes involved, which are, e.g., required for safety. These properties depend on pressure, temperature, and salt concentration.¹⁶ H₂ technologies cover a wide range of operational conditions. For example, in underground H₂ storage sites, the pressure, temperature, and salt molality can be as high as 300 bar, 333 K, and 5 mol NaCl/kg H₂O, respectively.⁷ Typically, H₂O electrolyzers operate at atmospheric pressure, temperatures of ca. (348 to 372) K, and molalities of ca. (3 to 4) electrolyte/kg H₂O.^{17,18} Other types of electrolysis require much higher pressures and temperatures, i.e., up to 700 bar and 1400 K, respectively.^{19–21} Thus, to cover the conditions for important H₂ applications, the

interfacial tensions, self-diffusivities, and solubilities need to be available for a very wide range of pressures, temperatures, and salt concentrations.

Traditionally, these thermophysical properties are measured experimentally.^{22–24} Nevertheless, only a small number of experimental studies on the interfacial tension of H₂/pure H₂O^{22,25–28} is available, while only two studies report measurements of interfacial tension of H₂/aqueous solutions (with NaCl and NaCl+KCl).^{27,28} These experiments are performed by using the capillary rise²⁹ and the pendant drop^{25,27,28,30} techniques. Interfacial tensions of H₂/aqueous solutions are reported for temperatures up to 423 K, pressures up to 345 bar, and molalities of up to 5 mol (NaCl + KCl)/kg H₂O. As far as the solubility of H₂ in aqueous NaCl solutions is concerned, for an overview of the available experimental data the reader is referred to the works of Chabab et al.,³¹ Torin-Ollarves and Trusler,³² and Ansari et al.³³ Although a lot of experimental data are available for H₂ in pure H₂O, solubility measurements of H₂ in aqueous NaCl solutions are scarce, and in many cases conflicting.^{23,31,34–38} The two main sources of

Special Issue: In Honor of Gabriele Sadowski

Received: November 12, 2022

Accepted: December 23, 2022

experimental data of solubilities of H_2 in aqueous solutions at concentrations above 1 mol NaCl/kg H_2O , at temperatures above 300 K, and at pressures above 10 bar by Torin-Ollarves and Trusler,³² and Chabab et al.³¹ show conflicting results as the measured solubilities differ by ca. 30%. For the self-diffusivity of H_2 in H_2O , experimental data are available^{24,39–46} but mostly at atmospheric pressure and for limited temperatures below 340 K. Similarly to the solubilities, the experimental measurements also differ by up to 70%. To the best of our knowledge, no experimental data are available for the self-diffusivity of H_2 in aqueous NaCl solutions.

Based on the available experimental data, it is evident that only a limited range of the required interfacial tensions, solubilities, and self-diffusivities of the $H_2/H_2O/NaCl$ system has been measured, while in some cases, there are significant discrepancies between the data reported from different sources. The reason for the scarcity of and deviation in the data may be that experimental measurements are rather challenging and expensive to perform, especially at high pressures and temperatures. To this end, a widely used complementary approach for obtaining thermophysical data is molecular simulation, especially at conditions which are challenging for experimental measurements.

Numerous studies have used Molecular Dynamics (MD) to compute the interfacial tension of gases (e.g., CO_2 , CH_4) and liquids (e.g., hydrocarbons) in contact with H_2O (pure or saline).^{47–57} However, no molecular simulation studies on the interfacial tension of H_2 and aqueous solutions are available. MD simulations have also been performed to compute self-diffusivities (i.e., self-diffusion coefficients) of H_2 in pure H_2O .^{58–62} Recently, Tsimpanogiannis et al.⁶⁰ reported such data for pressures in the range of (1 to 2000) bar and temperatures in the range of (275 to 975) K spanning vapor, liquid, and supercritical H_2O . The Marx,⁶³ Vrabec,⁶⁴ Buch,⁶⁵ Hirschenfelder,⁶⁶ Cracknell,⁶⁷ and Silvera-Goldman⁶⁸ H_2 force fields were used in combination with the TIP4P/2005⁶⁹ H_2O force field. The Buch⁶⁵ and Vrabec⁶⁴ H_2 force fields were shown to yield the best agreement with experimental data. In contrast, self-diffusivities of H_2 in aqueous NaCl solutions computed from MD simulations have not yet been reported, while there are a few studies available reporting computations of self-diffusivities of CO_2 in aqueous NaCl solutions.^{70–73} Lopez-Lazaro et al.⁷⁴ have computed solubilities of H_2 in aqueous NaCl solutions using Monte Carlo (MC) simulations for molalities up to a maximum of 2 mol NaCl/kg H_2O . To the best of the authors' knowledge, this was the only molecular simulation study on H_2 solubilities in aqueous NaCl solutions. Molecular simulations have been used for computing solubilities of other gases (e.g., CO_2 , CH_4) in water and aqueous NaCl solutions.^{52,57,75–77}

Despite the urgency and importance of reliable data of interfacial tension of H_2 in contact with aqueous NaCl solutions, self-diffusivity of H_2 in aqueous NaCl solutions, and solubility of H_2 in aqueous NaCl solutions, only very limited experimental and simulation studies are available. The objective of this work is to generate reliable data for these properties for a wide range of conditions relevant to H_2 technologies, such as underground H_2 storage and H_2O electrolysis. We present new data sets of (a) interfacial tensions of H_2 and aqueous NaCl solutions for temperatures, pressures, and molalities of (298 to 523) K, (1 to 600) bar, and (0 to 6) mol NaCl/kg H_2O , respectively, (b) self-diffusivities of H_2 in aqueous NaCl solutions for temperatures, pressures, and

molalities of (298 to 723) K, (1 to 1000) bar, and (0 to 6) mol NaCl/kg H_2O , respectively, and (c) solubilities of H_2 in aqueous NaCl solutions for temperatures, pressures, and molalities of (298 to 363) K, (1 to 1000) bar and (0 to 6) mol NaCl/kg H_2O , respectively. The interfacial tensions and self-diffusivities are computed using MD simulations, and the solubilities are computed using CFCMC^{78–80} simulations. Densities and viscosities of the aqueous NaCl solutions are also computed for a wide range of conditions and are compared to available experimental data. The TIP4P/2005⁶⁹ force field is used for H_2O , the Madrid-2019⁸¹ force field for NaCl, and the Vrabec⁶⁴ and Marx⁶³ force fields are used for H_2 . A modified version of the Madrid-2019 force field by Vega and co-workers⁸² (i.e., the Madrid-Transport^{77,82}), optimized for viscosities of aqueous NaCl solutions for salinities up to the experimental solubility limit, is also used.

The paper is structured as follows. Details of the force fields used and the molecular simulation techniques are given in section 2. In section 3, the computed interfacial tensions, viscosities, densities, self-diffusivities, and solubilities obtained are presented and compared with experimental data when possible. Finally, concluding remarks are presented in section 4. All data computed in this study are provided in a tabulated format as Supporting Information.

2. METHODOLOGY

2.1. Force Fields. The four-site TIP4P/2005⁶⁹ force field is used to model H_2O . Previous studies have shown that this force field can accurately capture thermodynamic, transport, and interfacial properties of pure H_2O and $H_2O/NaCl$ solutions in contact with gases for a wide range of conditions.^{47,49,60,83–88} For the Na^+ and Cl^- ions, the Madrid-2019⁸¹ force field is used, which is parametrized for the TIP4P/2005 H_2O model.⁸⁹ A new version of the Madrid-2019 force field (i.e., Madrid-Transport force field^{77,82}) is currently being developed by Vega and co-workers,⁸² which performs better for transport properties, especially at high NaCl molalities. The difference of Madrid-Transport from Madrid-2019 is that ion charges are scaled by 0.75 instead of 0.85, and the Lennard-Jones (LJ) parameters are slightly altered. Interfacial tensions and self-diffusivities are computed using the single-site Vrabec⁶⁴ H_2 force field, while for the solubilities of H_2 in the aqueous NaCl solutions the three-site Marx⁶³ model is used. Tsimpanogiannis et al.⁸⁴ showed that the Vrabec⁶⁴ H_2 force field yields very accurate self-diffusivities of H_2 in pure TIP4P/2005 H_2O . The solubilities computed using the Vrabec⁶⁴ force field deviate from experimental data of H_2 in pure water by ca. 50%. In sharp contrast, the solubilities computed using the Marx⁶³ force field show excellent agreement with experimental data. A comparison of the solubilities computed using the Marx and Vrabec force fields in pure TIP4P/2005 H_2O are listed in Table S1 and shown in Figure S1 of the Supporting Information. At low temperatures, H_2 exhibits quantum effects which can be accounted for by using potentials such as the Feynman-Hibbs effective interaction potential.^{90–92} At the temperatures considered in this work (i.e., 298 K and above) these quantum effects can be neglected.⁹³ All force field parameters are listed in Tables S2–S5 in the Supporting Information. A list of the chemical formulas, CAS numbers, and force fields of all species studied here is shown in Table 1.

2.2. Molecular Simulation Details. **2.2.1. MD Simulations.** The MD simulations are used to calculate (a) the

Table 1. Details of All the Species Simulated in This Work

Component	Chemical formula	CAS number	Force field
Water	H ₂ O	7732-18-5	TIP4P/2005 ⁶⁹
Hydrogen	H ₂	133-74-0	Vrabc64
Hydrogen	H ₂	133-74-0	Marx ⁶³
Sodium	Na ⁺	7440-23-5	Madrid-2019 ⁸¹
Sodium	Na ⁺	7440-23-5	Madrid-Transport ^{77,82}
Chloride	Cl ⁻	7782-50-5	Madrid-2019 ⁸¹
Chloride	Cl ⁻	7782-50-5	Madrid-Transport ^{77,82}

interfacial tensions of H₂ in contact with aqueous NaCl solutions, (b) self-diffusivities of H₂ in aqueous NaCl solutions, (c) densities, and (d) viscosities of aqueous NaCl solutions. For all MD simulations, the Large-scale Atomic/Molecular Massively Parallel Simulator (LAMMPS)⁹⁴ is used (version 29 Sep 2021). For the integration of the equations of motion, the velocity-Verlet algorithm is used with a time step of 1 fs. The bond length and bending angle of H₂O are fixed using the SHAKE algorithm.^{94,95} The intermolecular interactions are described by Lennard-Jones and Coulombic interaction potentials. The Lorentz–Berthelot combining rules⁹⁶ are used for interactions between different types of molecules, with the exception of Na⁺–H₂O, Na⁺–Cl⁻, and Cl⁻–H₂O LJ interactions as specified in Table S5. Long-range electrostatic energies are computed using the particle–particle particle–mesh (PPPM) method^{97,98} with a relative error⁹⁹ of 10⁻⁵. The temperature and pressure are regulated by the Nosé–Hoover thermostat and barostat.⁹⁷ Initial configurations are created using the PACKMOL software.¹⁰⁰ Periodic boundary conditions are imposed in all directions. All MD simulations for a specific set of conditions are repeated 5 times using different initial velocity distributions from which the average quantities are calculated. The reported uncertainties are standard deviations from the results of these 5 simulations.

2.2.2. Computation of Interfacial Tension. The following procedure is used for computing the interfacial tensions: An initial configuration is created by combining separately equilibrated bulk phases of aqueous sodium chloride solutions and H₂ gas. An equilibration run of 5 ns is carried out in the *NPT* ensemble using anisotropic pressure coupling, i.e., only the *z*-direction of the simulation box is allowed to fluctuate. The last 2 ns of the equilibration run are used to calculate the average simulation box dimensions, which are used for an equilibration run of 3 ns in the *NVT* ensemble. Next, production runs of 2 ns are carried out for computing the interfacial tension. In all simulations, 2088 H₂O molecules are used. Depending on the pressure, the number of H₂ molecules varied between 64–640. 0–188 Na⁺ and Cl⁻ ions are used, depending on the molality. The exact numbers of species along with the simulation box sizes for all simulations are listed in Table S6 of the Supporting Information. A cutoff radius of 12 Å is used for the short-range LJ and short-range electrostatic energies. Because the system is inhomogeneous, analytic corrections were not used. Instead, long-range LJ and electrostatic interactions are computed using the Particle–Particle Particle–Mesh (PPPM) method.^{97,98,101} For the real and reciprocal space computations for the dispersion part of the PPPM method the desired accuracies are set to 0.0001 and 0.002, respectively. A relative error of 10⁻⁵ is used for the long-range electrostatic energies. The adequacy of the PPPM method for computing the LJ interactions was recently

validated by Salehi et al.¹⁰² in interfacial MD simulations of deep eutectic solvents with water.

Figure 1 (top panel) shows a typical MD simulation snapshot at *T* = 343 K, *P* = 100 bar, and *m* = 3 mol NaCl/kg

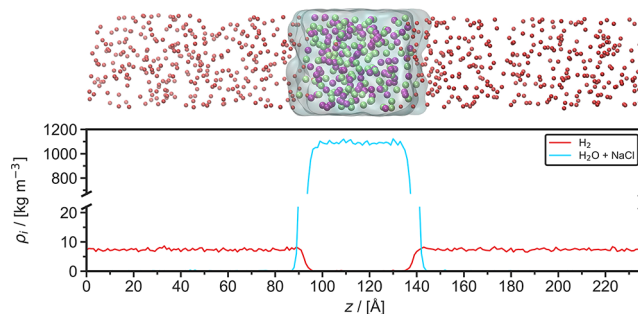


Figure 1. Top: Typical snapshot from a Molecular Dynamics simulation used to calculate the interfacial tension of H₂ and an aqueous NaCl solution (3 mol NaCl/kg H₂O) at 343 K and 100 bar. H₂ molecules are represented by red spheres, Na⁺ and Cl⁻ are represented by purple and green spheres, respectively, H₂O is represented by the transparent blue surface. Bottom: Density profile in the *z*-direction of H₂ and the aqueous NaCl solution of the same simulation, averaged over 1 ns. *z* is the direction perpendicular to the interface.

H₂O. The bulk liquid H₂O phase containing the Na⁺ and Cl⁻ ions, which is shown as the transparent blue surface, occupies a domain of ca. 40 × 40 × 40 Å³ in the middle of the simulation box. H₂ gas is in contact with the liquid phase from both sides, in the *z*-direction. This creates two H₂/H₂O interfaces perpendicular to the *z*-direction. The density profile of this system, averaged over 1 ns, is shown in Figure 1 bottom panel.

The interfacial tension γ is calculated from the principal components of the diagonal elements of the stress tensor (P_{zz} , P_{xx} , and P_{yy}):¹⁰³

$$\gamma = \frac{1}{2}h_z \left[P_{zz} - \frac{1}{2}(P_{xx} + P_{yy}) \right] \quad (1)$$

where h_z is the simulation cell length in the *z*-direction.

2.2.3. Computation of Self-Diffusivities and Viscosities. The scheme used for computing self-diffusivities and viscosities follows from ref 104. Initially, energy minimization of the system is performed, followed by equilibration runs in the *NPT* and *NVT* ensembles for 1–2 ns. Next, production runs in the *NVT* ensemble for 10 ns are carried out. The system consists of 700 H₂O molecules, 2 H₂ molecules, and 0–76 Na⁺ and Cl⁻ ions, depending on the molality. The exact numbers of species used for every state point are provided in Table S7 of the Supporting Information. A cutoff radius of 10 Å is used for Lennard-Jones and electrostatic interactions. Analytic tail corrections for energies and pressures are applied.

To compute the self-diffusivities and the shear viscosities, the OCTP plugin¹⁰⁴ in LAMMPS is used. In this plugin, the Einstein relations are used in combination with the order-*n* algorithm⁹⁷ as implemented by Dubbeldam et al.¹⁰⁵ Self-diffusivity D_i of species *i* is computed based on the mean-squared displacements using

$$D_i = \lim_{t \rightarrow \infty} \frac{1}{6N_i t} \left\langle \sum_{j=1}^{N_i} (\mathbf{r}_{j,i}(t) - \mathbf{r}_{j,i}(0))^2 \right\rangle \quad (2)$$

where $r_{j,i(t)}$ is the position vector of the j th molecule of species i at time t and N_i is the number of molecules of species i . All self-diffusivities in this work are corrected for finite-size effects using the Yeh-Hummer equation:^{106–108}

$$D = D_i + \frac{k_B T \xi}{6\pi\eta L} \quad (3)$$

where D is the finite-size corrected self-diffusivity, T is the temperature in K, ξ is a dimensionless constant equal to 2.837298, η is the shear viscosity from eq 4, and L is the simulation box length. In this work, the finite-size correction magnitude was ca. 5–10% of the computed self-diffusivities.

Shear viscosity η is computed from

$$\eta = \lim_{t \rightarrow \infty} \frac{1}{10 \cdot 2t} \frac{V}{k_B T} \left\langle \sum_{\alpha\beta} \left(\int_0^t P_{\alpha\beta}^{\text{os}}(t') dt' \right)^2 \right\rangle \quad (4)$$

where

$$P_{\alpha\beta}^{\text{os}} = \frac{P_{\alpha\beta} + P_{\beta\alpha}}{2} - \delta_{\alpha\beta} \left(\frac{1}{3} \sum_k P_{kk} \right) \quad (5)$$

where V is the volume of the system, k_B is the Boltzmann constant, $P_{\alpha\beta}^{\text{os}}$ denotes the components of the traceless pressure tensor, $\delta_{\alpha\beta}$ is the Kronecker delta, and $\langle \dots \rangle$ indicates an ensemble average. The computation of η does not depend on the size of the system.^{109–111}

2.2.4. Computation of Solubilities. Continuous Fractional Component Monte Carlo^{78–80} simulations in the isobaric–isothermal (CFCNPT) ensemble are used to compute solubilities and excess chemical potentials of H_2 in NaCl solutions. The open-source Brick-CFCMC software^{78,112,113} is used for all simulations. A 10 Å cutoff radius is used for both the LJ and Coulombic interactions. The Ewald summation with a relative precision of 10^{-6} is used for the electrostatics. Analytic tail corrections for energies and pressures are applied.⁹⁷ The infinite dilution excess chemical potential of H_2 can be computed using a single “fractional” molecule of H_2 . Fractional molecules have their interactions scaled with a continuous order parameter λ .^{78,93} In CFCNPT simulations, λ ranges from 0 to 1. $\lambda = 0$ indicates that the fractional molecule does not interact with the surrounding molecules/atoms (i.e., the fractional molecule behaves as an ideal gas molecule), and $\lambda = 1$ corresponds to full interactions. For the specifics regarding the scaling of the interactions the reader is referred elsewhere.^{114–116} To improve the sampling in the λ -space, a biasing weight function ($W(\lambda)$) is created using the Wang–Landau algorithm.^{117,118} This biasing weight function is used to ensure a flat probability distribution in the λ -space ($p_{\text{obs}}(\lambda)$). To compute the probability of occurrence of each λ value, a histogram with 100 bins is used. The Boltzmann averaged probability distributions of λ ($p(\lambda)$) can be computed using^{77,119}

$$p(\lambda) = \frac{\langle p_{\text{obs}}(\lambda) \exp[-W(\lambda)] \rangle}{\langle \exp[-W(\lambda)] \rangle} \quad (6)$$

The Boltzmann sampled probability distribution of λ ($p(\lambda)$) can be related to the infinite dilution chemical potential (μ^{ex}) using^{77,78,119}

$$\mu^{\text{ex}} = -k_B T \ln \frac{p(\lambda = 1)}{p(\lambda = 0)} \quad (7)$$

where $p(\lambda = 1)$ and $p(\lambda = 0)$ are the Boltzmann averaged probability distributions of λ at 1 and 0, respectively.

Five $\times 10^5$ equilibration cycles, and 5×10^5 production cycles are performed for all simulations. A cycle contains N number of trial moves, with N being the total number of molecules, with a minimum of 20. The following probabilities are used for selecting the trial moves: 35% translations, 29% rotations, 1% volume changes, 25% λ changes, and 10% reinsertions of the fractional molecules at random locations inside the simulation box. The maximum displacements for molecule translations, volume changes, rotations, and λ changes are adjusted to obtain ca. 50% acceptance. Another method that can be used to compute μ^{ex} is the Widom’s Test Particle Insertion method (WTPI).^{96,97,120,121} In dense fluid phases WTPI yields inaccurate results compared to the CFCMC method as successful insertion of test particles is a highly unlikely event due to the significant potential energy increase in case of overlap with other particles.^{78,122}

The solubilities of H_2 in aqueous NaCl solutions are computed at temperatures in the range (298 to 363) K and at H_2 partial pressures of 1, 10, 100, 400, and 1000 bar. At H_2 partial pressures of 1 and 10 bar, the H_2 solubilities are computed using Henry coefficients (H):

$$H = \lim_{f_i \rightarrow 0} \frac{f_i}{\langle \rho_{\text{H}_2, \text{L}} \rangle / \rho_0} \quad (8)$$

where f_i is the fugacity of H_2 in the gas phase, $\langle \rho_{\text{H}_2, \text{L}} \rangle$ is the average number density of H_2 in the aqueous solution in units of $1/\text{m}^3$, and ρ_0 is a reference number density in the same unit as $\rho_{\text{H}_2, \text{L}}$ (set to 1 molecule per m^3).¹¹⁹ At H_2 partial pressures of 1 and 10 bar, the fugacity coefficient of H_2 is assumed to be 1 (i.e., the fugacity of H_2 is equal to the partial pressure of H_2). The validity of eq 8 at H_2 partial pressures of 1–100 bar is discussed in Figure S3 of the Supporting Information. From the MC simulations, H can be computed using¹¹⁹

$$H = \rho_0 k_B T \exp \left[\frac{\mu_{\text{H}_2, \text{L}}^{\text{ex}}}{k_B T} \right] \quad (9)$$

where $\mu_{\text{H}_2, \text{L}}^{\text{ex}}$ is the infinite dilution chemical potential of H_2 in the aqueous solution. A single fractional molecule of H_2 , 300 H_2O molecules, and varying number of NaCl molecules depending on the molality (ranging from 0 to 6 mol NaCl/kg H_2O) are used to compute $\mu_{\text{H}_2, \text{L}}^{\text{ex}}$. The exact numbers of ions used for each molality are listed in Table S8 of the Supporting Information. To calculate solubilities of H_2 in aqueous NaCl solutions at pressures of 100, 400, and 1000 bar, the chemical potentials of H_2 in the liquid and in the gas phase are equated at constant pressure and temperature. The chemical potential of H_2 in the gas phase ($\mu_{\text{H}_2, \text{G}}$) is equal to⁹⁷

$$\mu_{\text{H}_2, \text{G}} = \mu_{\text{H}_2}^0 + k_B T \ln \left(\frac{\langle \rho_{\text{H}_2, \text{G}} \rangle}{\rho_0} \right) + \mu_{\text{H}_2, \text{G}}^{\text{ex}} \quad (10)$$

where $\mu_{\text{H}_2}^0$ is the reference state of the chemical potential, $\langle \rho_{\text{H}_2, \text{G}} \rangle$ is the average number density of H_2 in the gas phase in units of $1/\text{m}^3$, and $\mu_{\text{H}_2, \text{G}}^{\text{ex}}$ is the excess chemical potential of H_2 in the gas phase. At pressures above 100 bar and at temperatures between (298 to 363) K, the gas phase contains very few H_2O molecules (a H_2O mole fraction below 0.01).⁹³

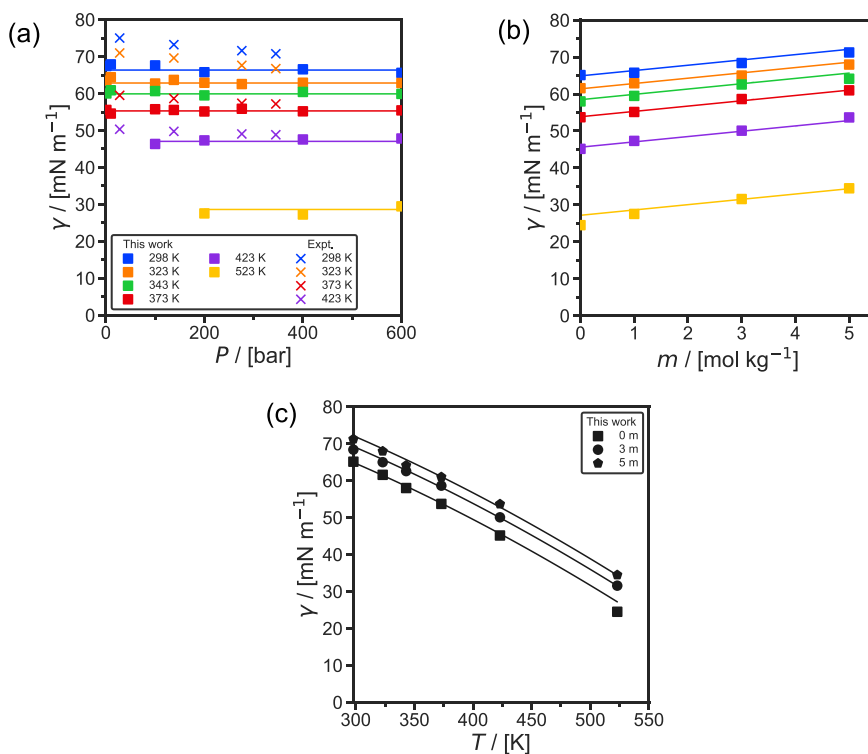


Figure 2. MD results of interfacial tension γ of H_2 and aqueous NaCl solutions using the NaCl Madrid-2019⁸¹ force fields, the TIP4P/2005⁶⁹ H_2O force field, and the Vrabec⁶⁴ H_2 force field (a) as functions of pressure P for temperatures in a range of (298 to 523) K with a molality m of 1 mol NaCl/kg H_2O in combination with the experimental results of Hosseini et al.,²⁷ (b) as functions of molality at a pressure of 200 bar of the solution for similar temperatures, and (c) as functions of temperature at a pressure of 200 bar and molalities of (0 to 6) mol NaCl/kg H_2O . The statistical uncertainties are comparable to or smaller than the symbols and can be found in Table S9 of the Supporting Information. The error bars have been omitted for clarity. The solid lines represent fits using eq 13 for temperatures in the range of (298 to 523) K.

$\mu_{\text{H}_2,\text{G}}^{\text{ex}}$ is calculated in separate CFCNPT simulations, containing a single fractional molecule of H_2 , and 300 H_2 molecules in the gas phase. At conditions where the gas phase is nonideal and the H_2O content in the gas phase is not negligible (i.e., temperatures above 363 K and pressures above 100 bar), Gibbs ensemble simulations can be performed to simulate the gas and the liquid phase simultaneously.⁹³ These simulations are beyond the scope of this work. The chemical potential of H_2 in the liquid phase ($\mu_{\text{H}_2,\text{L}}$) is equal to⁹⁷

$$\mu_{\text{H}_2,\text{L}} = \mu_{\text{H}_2}^0 + k_{\text{B}}T \ln \left(\frac{\langle \rho_{\text{H}_2,\text{L}} \rangle}{\rho_0} \right) + \mu_{\text{H}_2,\text{L}}^{\text{ex}} \quad (11)$$

$\langle \rho_{\text{H}_2,\text{L}} \rangle$ can be computed by equating eq 10 and eq 11. The mole fractions of H_2 (x_{H_2}) in aqueous NaCl solutions are computed using

$$x_{\text{H}_2} = \frac{\langle \rho_{\text{H}_2,\text{L}} \rangle \langle V \rangle}{N_{\text{H}_2\text{O}} + N_{\text{NaCl}} + \langle \rho_{\text{H}_2,\text{L}} \rangle \langle V \rangle} \quad (12)$$

where $\langle V \rangle$ is the average volume of the simulation box, computed in the CFCNPT ensemble. $N_{\text{H}_2\text{O}}$ and N_{NaCl} are the numbers of H_2O and NaCl molecules in the simulation box, respectively. For each condition (concentration, temperature, and pressure), 20 independent simulations are performed. These 20 simulations are divided into 5 blocks from which the Boltzmann sampled probability distributions of λ ($p(\lambda)$) are averaged. The averaged distributions ($p(\lambda)$) of all blocks are

used to compute mean values and standard deviations for the excess chemical potentials and solubilities of H_2 .

3. RESULTS AND DISCUSSION

3.1. Interfacial Tensions. Figure 2 shows the computed interfacial tensions of $\text{H}_2/\text{H}_2\text{O}/\text{NaCl}$ as a function of pressure (Figure 2a), molality (Figure 2b) at temperatures in the range of (298 to 523) K, and as a function of temperature (Figure 2c) for molalities in the range of (0 to 6) mol NaCl/kg H_2O . Tabulated raw data of the interfacial tension along with their statistical uncertainties are listed in Table S9 of the Supporting Information. Figure 2a and 2c also show the available experimental data from Hosseini et al.²⁷ For the whole range of conditions a close agreement with the experimental results is found. The MD results differ on average 6.4% from the experimental values. The simulations at 523 K cannot be directly validated due to lack of experimental data.

The interfacial tensions computed in this work are fitted to an engineering equation:

$$\gamma = c_1 + c_2 m + c_3 T^{c_4} \quad (13)$$

where c_1 , c_2 , c_3 , and c_4 are fitting parameters, which are listed in Table 2. Equation 13 is valid for temperatures, pressures, and molalities of (298 to 523) K, (1 to 600) bar, and (0 to 6) mol NaCl/kg H_2O , respectively. The results of this engineering equation are shown as solid lines in Figure 2. Equation 13 is a very good fit to MD results, and can be used for calculating values at a specific combination of conditions in a fast and reliable way.

Table 2. Parameters of eq 13 for Predicting Interfacial Tension of H₂ in Contact with Aqueous NaCl Solutions^a

$c_1/[\text{mN/m}]$	89.6
$c_2/[(\text{mN}\cdot\text{kg}_{\text{H}_2\text{O}})/(\text{m}\cdot\text{mol}_{\text{NaCl}})]$	1.44
$c_3/[\text{mN}/(\text{m}\cdot\text{K}^{1.65})]$	-2.04×10^{-3}
$c_4/[-]$	1.65

^aValues obtained using the NaCl Madrid-2019⁸¹ force fields, TIP4P/2005⁶⁹ H₂O force field, and Vrabec⁶⁴ H₂ force field. These parameters are valid for NaCl molalities of (0 to 6) mol NaCl/kg H₂O, temperatures of (298 to 523) K, and pressures of (1 to 600) bar.

As shown in Figure 2a, no significant pressure dependence of interfacial tension is observed. The data of experimental studies also show no significant or small pressure dependences.^{22,25,27,28} In particular, Higgs et al.²⁸ did not observe a significant pressure dependence for H₂ in contact with aqueous NaCl solutions. Other studies observed a small decrease in interfacial tension of H₂ and pure H₂O^{22,25,27} and H₂ and aqueous (NaCl+KCl) solutions.²⁷ Interestingly, the pressure dependence of H₂/H₂O interfacial tension is small compared to the CO₂/H₂O^{123–125} and CH₄/H₂O^{51,126,127} systems. This is because the interfacial tension is related to the density difference between the two phases.¹⁶ The change in density difference between H₂ and H₂O is very small at varying pressures because the density of H₂ is very low in comparison to H₂O, and H₂O is almost incompressible at these pressures.

As shown in Figure 2b, the interfacial tension increases linearly with solution molalities, in agreement with the available experimental data.²⁷ This behavior is also observed for other gases such as CO₂ and CH₄.^{128–130} This increase is mainly due to the increased density of saline H₂O compared to pure H₂O as well as the arrangement of cations and anions at the interface.^{129,131–135} The hydrogen bond network of H₂O is strengthened by cations,^{132–134} while anions cause the opposite effect.^{132–134} Therefore, cations are absorbed into the bulk phase while anions are depleted from the bulk phase. This phenomenon can be observed in Figure S2 of the Supporting Information, where it is shown that the number density of Cl[−] ions at the interface is higher than Na⁺ ions, and Na⁺ ions are drawn into the bulk phase. The strengthening of the hydrogen bond network of H₂O leads to an increase in interfacial tension.^{129,131}

In Figure 2c, a nonlinear decrease of interfacial tension with temperature can be observed. This is in line with the

experimental data of Chow et al.²⁵ In sharp contrast, Hosseini et al.²⁷ reported a linear decrease of interfacial tension with temperature. The fact that interfacial tension depends nonlinearly on the density difference between the two phases in contact¹⁶ combined with the nonlinear effect of temperature on the density difference between H₂ and H₂O, results in the expectation that the interfacial tension is also nonlinearly related to temperature. Therefore, the observed nonlinear relationship between interfacial tension and temperature in our results is expected.

3.2. Viscosities and Densities. Figure 3 shows the computed densities and viscosities of aqueous NaCl solutions as functions of NaCl molalities at 298 and 343 K. The densities are computed from the average volume calculated from the NPT ensemble. Equation 4 is used to compute the viscosities. Densities and viscosities of aqueous NaCl solutions have a weaker dependence on pressure (in the range of 0–1000 bar) compared to temperature and NaCl molalities. Figures S4 and S5 in the Supporting Information show the densities and the viscosities as functions of pressure. The results for the Madrid-2019⁸¹ and the Madrid-Transport^{77,82} NaCl force fields are shown in Figure 3. Laliberté¹³⁶ and Laliberté and Cooper¹³⁷ developed models on the basis of experimental data for viscosities and densities, respectively. These fits are shown in Figure 3. The raw data of these properties, as well as their statistical uncertainties, are listed in Table S10 of the Supporting Information. Both the Madrid-2019⁸¹ and Madrid-Transport^{77,82} capture the experimental data of density very accurately (within 1%). As shown in Figure 3a, the Madrid-Transport^{77,82} force field yields a better agreement with the experimental data of viscosity compared to the Madrid-2019⁸¹ force field. The discrepancy between the two force fields starts at molalities above 2 mol NaCl/kg H₂O. The viscosities computed using the Madrid-2019 force field deviate on average ca. 20% from the experimental data, while this deviation is only ca. 3% when the Madrid-Transport force field is used. Based on the excellent performance of Madrid-Transport in reproducing experimental viscosities, which is necessary for reliable diffusivity predictions,¹³⁸ only this force field was used for computing the self-diffusivities of H₂ in NaCl solutions.

3.3. Self-Diffusivities of H₂. Figure 4 shows the computed finite-size corrected self-diffusivities of H₂ in aqueous NaCl solutions as a function of (a) pressure, (b) NaCl molality, and

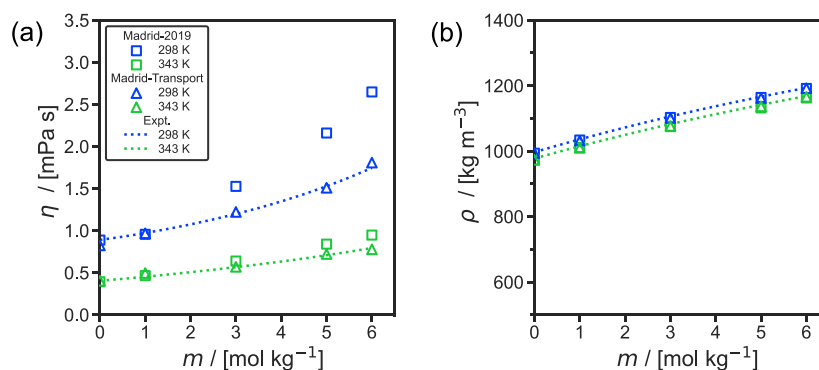


Figure 3. Computed (a) viscosities η and (b) densities ρ of aqueous NaCl solutions as a function of molality m (mol NaCl/kg H₂O) at a pressure of 1 bar and temperatures of 298 and 343 K. The fit to the experimental data is created by (a) Laliberté¹³⁶ and (b) Laliberté and Cooper.¹³⁷ The statistical uncertainties can be found in Table S10 of the Supporting Information. The error bars are smaller or comparable to the symbol size and have been omitted for clarity.

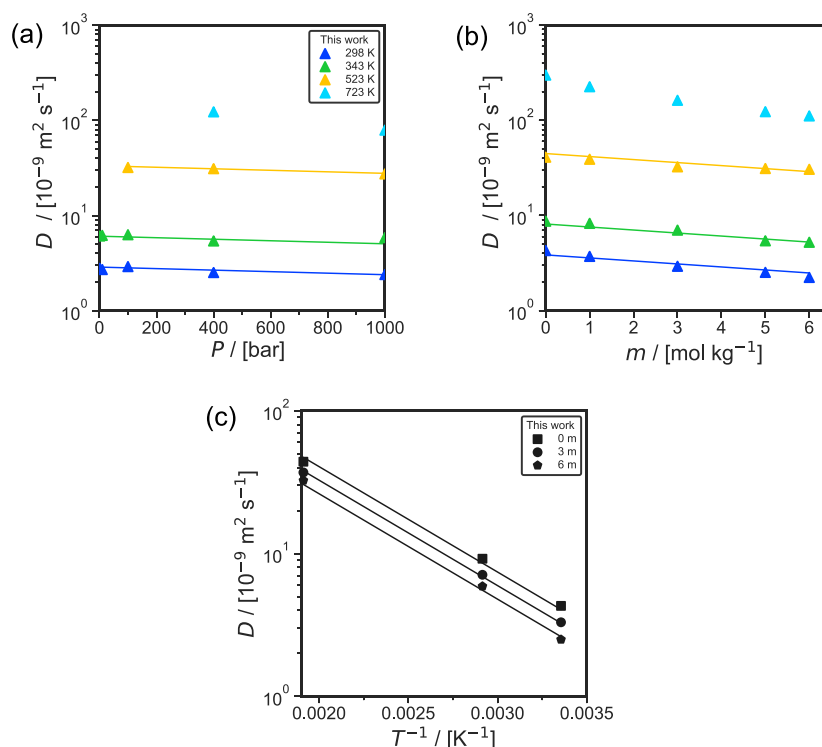


Figure 4. Computed finite-size corrected self-diffusivities (D) of H_2 in aqueous NaCl solutions (a) with a molality (m) of 5 mol NaCl/kg H_2O solution as a function of pressure P for temperatures of (298 to 723) K, (b) at a pressure of 400 bar as a function of m of the solution for the similar temperatures, and (c) as a function of the reciprocal temperature at a pressure of 100 bar. The results are obtained using the NaCl Madrid-Transport^{77,82} force fields, TIP4P/2005⁶⁹ H_2O force field, and Vrabec⁶⁴ H_2 force field. The statistical uncertainties are comparable to or smaller than the symbols and can be found in Table S11 of the Supporting Information. The solid lines are fits calculated using eq 14 for temperatures of (298 to 523) K. Data points at a temperature of 723 K and a pressure of 400 bar are excluded from the fit because H_2O is supercritical at these conditions.

(c) temperature. These simulation are performed with the Madrid-Transport^{77,82} force field for NaCl, the TIP4P/2005⁶⁹ H_2O , and the Vrabec⁶⁴ force field for H_2 . All the self-diffusivities of H_2 computed in this work are listed in Tables S11 and S12 of the Supporting Information. Simulations using the Madrid-2019⁸¹ NaCl force field are performed for comparison. These data are shown in Table S12 of the Supporting Information.

The self-diffusivities of H_2 shown in Figure 4 are fitted to an engineering correlation:

$$D = c_1 \exp \left[c_2 m + c_3 \left(\frac{1}{T} \right) + c_4 P \right] \quad (14)$$

where c_1 , c_2 , c_3 , and c_4 are fitting parameters, which are listed in Table 3. As shown in Figure 4, this correlation provides an excellent fit for the MD results. Note that eq 14 is only valid for conditions at which H_2O is in the liquid phase, and therefore, data points at temperatures of 723 K or higher are excluded as the solution is in the supercritical phase. In this work, self-diffusivities for temperatures of 723 K and pressures lower than 400 bar are not calculated, because at those conditions, H_2O is in the gas phase. Equation 14 is an empirical model.

In Figure 4a a weak pressure dependence of the self-diffusivities of H_2 is observed. The logarithm of the self-diffusivities decays linearly with respect to variations in pressure, similarly to what is reported by Tsimpanogiannis et al.⁸⁴ The pressure dependence of the self-diffusivities of H_2 is more significant at 723 K (Figure 4a) as the solution is more

Table 3. Parameters of eq 14 for Predicting the Computed Finite-Size Corrected Self-Diffusivities D of H_2 in Aqueous NaCl Solutions^a

$c_1/[\text{m}^2/\text{s}]$	1.24×10^{-6}
$c_2/[(\text{mol}_{\text{NaCl}}/\text{kg}_{\text{H}_2\text{O}})^{-1}]$	-7.29×10^{-2}
$c_3/[\text{K}]$	-1.70×10^3
$c_4/[\text{bar}^{-1}]$	-1.84×10^{-4}

^aValues obtained using the NaCl Madrid-Transport^{77,82} force fields, the TIP4P/2005⁶⁹ H_2O force field, and the Vrabec⁶⁴ H_2 force field. These parameters are valid for NaCl molalities of (0 to 6) mol NaCl/kg H_2O , temperatures of (298 to 523) K, and pressures of (1 to 1000) bar. Note that eq 14 should only be used at conditions in which water is in the liquid state.

compressible at these conditions. As shown in Figure 4b, the logarithm of the self-diffusivities is also found to decay linearly with respect to variation in the NaCl molalities. Labiberte¹³⁶ has shown that the viscosities of aqueous NaCl solutions increase exponentially with respect to NaCl molalities. As the self-diffusivities of gases dissolved in liquids are inversely proportional to the viscosities of the solution,^{16,138} the self-diffusivities of H_2 are expected to decay exponentially with respect to the NaCl molalities. The computed self-diffusivities of H_2 follow an Arrhenius-type⁹⁷ relation with respect to variations in temperature ($D \propto \exp \left[\frac{c}{T} \right]$) as shown in Figure 4c. This behavior is also observed in literature for gases (e.g., O_2 , H_2) dissolved in aqueous solvents.^{60,86,139–141}

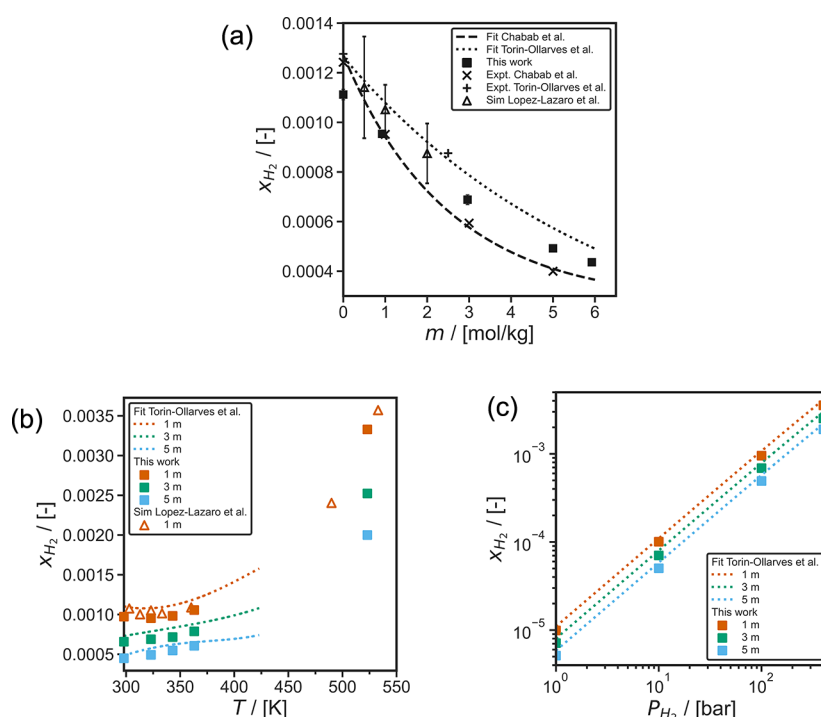


Figure 5. Computed solubilities of H₂ in aqueous NaCl solutions using the NaCl Madrid-2019 force field,⁸¹ TIP4P/2005⁶⁹ H₂O force field, and Marx⁶³ H₂ force field as functions of (a) NaCl molality (m) in units of mol NaCl/kg H₂O for a H₂ partial pressure of 100 bar, at 323 K, (b) temperature for a H₂ partial pressure of 100 bar, and (c) H₂ partial pressure at 323 K. The dashed lines represent the experimental correlation provided by Torin-Ollarves and Trusler,³² and the dotted lines represent the experimental correlation results of Chabab et al.³¹ The experimental data of Chabab et al.,³¹ and Torin-Ollarves and Trusler,³² and the simulation results of Lopez-Lazaro et al.⁷⁴ (converted from Henry constants) are also shown. The error bars of the simulations of this work are comparable (Figure 5a) or smaller than (Figure 5b and 5c) the symbol size.

3.4. Solubilities. In Figure 5, the solubilities of H₂ computed using CFCMC are shown as a function of (a) NaCl molality, (b) temperature, and (c) pressure. The computed solubilities are compared to the experimental measurements of Chabab et al.,³¹ Torin-Ollarves and Trusler,³² and their corresponding experimental correlations (also shown in Figure 5). The correlation of Torin-Ollarves and Trusler³² is based on the experimental measurements for NaCl molalities of 0 and 2.5 mol NaCl/kg H₂O, the experimental data by Wiebe and Gaddy,¹⁴² Wiebe et al.,¹⁴³ Kling and Maurer,¹⁴⁴ and Choudhary et al.¹⁴⁵ for H₂ solubility in pure H₂O, and the experiments by Crozier and Yamamoto³⁷ and Gordon et al.³⁸ for solubility of H₂ in saline solutions. Chabab et al.³¹ provide an extensive experimental data set and a correlation for H₂ solubilities at temperatures of (323 to 373) K, and NaCl molalities in the range of (0 to 5) mol/kg H₂O. Lopez-Lazaro et al.⁷⁴ obtained the Henry constants of H₂ in aqueous NaCl solutions for molalities up to 2 mol NaCl/kg H₂O using excess chemical potentials computed using the WTPI method.^{96,97,120,121} Using the Henry constants reported by Lopez-Lazaro et al.,⁷⁴ the solubilities of H₂ at a partial pressure of 100 bar are computed and shown in Figures 5a and 5b. The simulations of Lopez-Lazaro et al.⁷⁴ show large error bars (ca. 10–20%). This may be due to the use of the WTPI method,^{96,97,120,121} which requires a large number of MC cycles to obtain low standard deviations for excess chemical potentials in the liquid phase.^{74,78} The solubilities computed in this work using CFCMC simulations^{79,80,112,113} have uncertainties of less than 5%.

Figure 5a shows the decrease of the solubilities of H₂ at increasing molalities of NaCl (i.e., salting-out effect). The

salting-out of nonpolar gases (e.g., H₂, O₂, and CO₂) in the presence of salts such as NaCl, KCl, and KOH is a well observed phenomenon.^{57,77,135} As shown in Figure 5a, the models by Torin-Ollarves and Trusler³² and Chabab et al.³¹ agree for H₂ solubilities in pure H₂O and at NaCl molalities below 0.5 mol NaCl/kg H₂O. For NaCl concentrations higher than 0.5 mol NaCl/kg H₂O the two models predict different H₂ solubilities. The salting-out effect of H₂ observed in this work using the Madrid-2019⁸¹ Na⁺ and Cl⁻, TIP4P/2005⁶⁹ H₂O, and the Marx⁶³ H₂ force fields shows better agreement to the salting-out effect observed by Torin-Ollarves and Trusler³² as shown in Figure 5a. The correlation of Torin-Ollarves and Trusler³² also shows agreement with our simulations at H₂ partial pressures ranging from (1 to 400) bar in the temperature range (298 to 363) K, as shown in Figures 5b and 5c. Our simulation results also agree with the MC simulations by Lopez-Lazaro et al.⁷⁴ both for different NaCl molalities, and for different temperatures in the range of (298 to 523) K, even though the choice of the force fields for Na⁺, Cl⁻, and H₂ is different. Lopez-Lazaro et al.⁷⁴ have used the OPLS force field¹⁴⁶ for Na⁺, and Cl⁻, combined with the model by Darkim et al.¹⁴⁷ for H₂.

In Table S13 of the Supporting Information, we provide an extensive database for solubilities of H₂ at temperatures of (298 to 363) K, H₂ partial pressures of (1 to 1000) bar, and at NaCl molalities of (0 to 6) mol/kg H₂O. The solubilities of H₂ at partial pressures up to 100 bar are computed for a wider temperature range, i.e., (298 to 523) K. These data can be further used to test and train existing machine-learning models³³ or equations of state¹⁴⁸ for predicting H₂ solubilities

in saline solutions at conditions relevant to geological H₂ storage.

4. CONCLUSIONS

Molecular simulations are used to compute (a) interfacial tensions of H₂ and aqueous NaCl solutions for temperatures, pressures, and molalities of (298 to 523) K, (1 to 600) bar, and (0 to 6) mol NaCl/kg H₂O, respectively, (b) self-diffusivities of H₂ in aqueous NaCl solutions for temperatures, pressures, and molalities of (298 to 723) K, (1 to 1000) bar and (0 to 6) mol NaCl/kg H₂O, respectively, and (c) solubilities of H₂ in aqueous NaCl solutions for temperatures, pressures, and molalities of (298 to 363) K, (1 to 1000) bar, and (0 to 6) mol NaCl/kg H₂O, respectively. The simulations for computing H₂ self-diffusivities are also used to yield predictions for densities and viscosities of the NaCl solutions. The interfacial tensions and self-diffusivities are computed using MD simulations, and the solubilities are computed using CFCMC simulations. The H₂O TIP4P/2005⁶⁹ force field, the NaCl Madrid-2019⁸¹ force fields, and H₂ Vrabec⁶⁴ and Marx⁶³ force fields are used. In addition, a modified version of the Madrid-2019 force field (i.e., the Madrid-Transport^{77,82} force field) is used, which is optimized for transport properties of aqueous solutions. Our results are validated against the available experimental data, models, and simulations. Excellent agreement between the results and experimental data is found with deviations smaller than 10% for the vast majority of the data points. The results of the NaCl Madrid-Transport force field were in better agreement with experimental data for transport properties, while the Madrid-2019 force field was sufficiently accurate for interfacial tensions and solubilities. The new data are used to develop engineering equations for interfacial tension and self-diffusion capturing the effect of pressure, temperature, and solution molality.

■ ASSOCIATED CONTENT

SI Supporting Information

The Supporting Information is available free of charge at <https://pubs.acs.org/doi/10.1021/acs.jced.2c00707>.

Solubilities of H₂ in pure water; force field parameters; additional info MD and CFCMC simulations; raw data MD simulations for interfacial tensions; density and viscosity data; raw data MD simulations for self-diffusivities; raw data CFCMC simulations; solubilities of H₂ in pure water; density profile of Na⁺ and Cl⁻ of a MD simulation to calculate interfacial tensions; solubilities of H₂ in aqueous NaCl solution at H₂ partial pressures of 1–100 bar; densities of NaCl solutions; viscosities of NaCl solutions (PDF)

■ AUTHOR INFORMATION

Corresponding Author

O. A. Moulτος – *Engineering Thermodynamics, Process and Energy Department, Faculty of Mechanical, Maritime and Materials Engineering, Delft University of Technology, 2628CB Delft, The Netherlands*; orcid.org/0000-0001-7477-9684; Email: o.moulτος@tudelft.nl

Authors

W. A. van Rooijen – *Reservoir Engineering, Geoscience and Engineering Department, Faculty of Civil Engineering and*

Geosciences, Delft University of Technology, 2628CN Delft, The Netherlands

P. Habibi – *Engineering Thermodynamics, Process and Energy Department, Faculty of Mechanical, Maritime and Materials Engineering, Delft University of Technology, 2628CB Delft, The Netherlands*; *Department of Materials Science and Engineering, Faculty of Mechanical, Maritime and Materials Engineering, Delft University of Technology, 2628CD Delft, The Netherlands*

K. Xu – *Department of Materials Science and Engineering, Faculty of Mechanical, Maritime and Materials Engineering, Delft University of Technology, 2628CD Delft, The Netherlands*

P. Dey – *Department of Materials Science and Engineering, Faculty of Mechanical, Maritime and Materials Engineering, Delft University of Technology, 2628CD Delft, The Netherlands*; orcid.org/0000-0003-4679-1752

T. J. H. Vlught – *Engineering Thermodynamics, Process and Energy Department, Faculty of Mechanical, Maritime and Materials Engineering, Delft University of Technology, 2628CB Delft, The Netherlands*; orcid.org/0000-0003-3059-8712

H. Hajibeygi – *Reservoir Engineering, Geoscience and Engineering Department, Faculty of Civil Engineering and Geosciences, Delft University of Technology, 2628CN Delft, The Netherlands*

Complete contact information is available at:

<https://pubs.acs.org/10.1021/acs.jced.2c00707>

Author Contributions

[§]W.A.v.R. and P.H. contributed equally.

Notes

The authors declare no competing financial interest.

■ ACKNOWLEDGMENTS

Hadi Hajibeygi and Willemijn van Rooijen were sponsored by the Dutch National Science Foundation (NWO) Talent Programme ViDi Project “ADMIRE” (grant number 17509). This work was also sponsored by NWO Domain Science for the use of supercomputer facilities. Thijs J. H. Vlught acknowledges NWO-CW (Chemical Sciences) for a VICI grant. O. A. Moulτος gratefully acknowledges the support of NVIDIA Corporation with the donation of the Titan V GPU used for this research. The authors acknowledge Carlos Vega and Samuel Blazquez for sharing the Madrid-Transport force field parameters prior to publication and for stimulating scientific discussions.

■ REFERENCES

- (1) World Energy Outlook 2021. 2021; www.iea.org/weo (accessed: 10/10/2022).
- (2) United Nations, The Paris Agreement. 2015; https://treaties.un.org/pages/ViewDetails.aspx?src=TREATY&mtdsg_no=XXVII-7-d&chapter=27&clang=_en (accessed: 10/10/2022).
- (3) Johnston, B.; Mayo, M. C.; Khare, A. Hydrogen: the energy source for the 21st century. *Technovation* **2005**, *25*, 569–585.
- (4) Mahlia, T.; Saktisahdan, T.; Jannifar, A.; Hasan, M.; Matseelar, H. A review of available methods and development on energy storage; technology update. *Renewable Sustainable Energy Rev.* **2014**, *33*, 532–545.
- (5) Kovač, A.; Paranos, M.; Marciuš, D. Hydrogen in energy transition: A review. *Int. J. Hydrogen Energy* **2021**, *46*, 10016–10035.

- (6) Carden, P. O.; Paterson, L. Physical, chemical and energy aspects of underground hydrogen storage. *Int. J. Hydrogen Energy* **1979**, *4*, 559–569.
- (7) Zivar, D.; Kumar, S.; Foroozesh, J. Underground hydrogen storage: A comprehensive review. *Int. J. Hydrogen Energy* **2021**, *46*, 23436–23462.
- (8) Tarkowski, R. Underground hydrogen storage: Characteristics and prospects. *Renewable Sustainable Energy Rev.* **2019**, *105*, 86–94.
- (9) Hashemi, L.; Blunt, M.; Hajibeygi, H. Pore-scale modelling and sensitivity analyses of hydrogen-brine multiphase flow in geological porous media. *Sci. Rep.* **2021**, *11*, 1–13.
- (10) Ursúa, A.; Gandía, L. M.; Sanchis, P. Hydrogen production from water electrolysis: Current status and future trends. *Proc. IEEE* **2012**, *100*, 410–426.
- (11) Grigoriev, S. A.; Fateev, V. N.; Bessarabov, D. G.; Millet, P. Current status, research trends, and challenges in water electrolysis science and technology. *Int. J. Hydrogen Energy* **2020**, *45*, 26036–26058.
- (12) Pan, B.; Yin, X.; Ju, Y.; Iglauer, S. Underground hydrogen storage: Influencing parameters and future outlook. *Adv. Colloid Interface Sci.* **2021**, *294*, 102473.
- (13) Haug, P.; Koj, M.; Turek, T. Influence of process conditions on gas purity in alkaline water electrolysis. *Int. J. Hydrogen Energy* **2017**, *42*, 9406–9418.
- (14) Haug, P.; Kreitz, B.; Koj, M.; Turek, T. Process modelling of an alkaline water electrolyzer. *Int. J. Hydrogen Energy* **2017**, *42*, 15689–15707.
- (15) Zarghami, A.; Deen, N.; Vreman, A. CFD modeling of multiphase flow in an alkaline water electrolyzer. *Chem. Eng. Sci.* **2020**, *227*, 115926.
- (16) Poling, B. E.; Prausnitz, J. M.; O'Connell, J. P. *Properties of gases and liquids*, 5th ed.; McGraw-Hill Education: New York, 2001.
- (17) Zoulias, E.; Varkarakí, E.; Lymberopoulos, N.; Christodoulou, C. N.; Karagiorgis, G. N. A review on water electrolysis. *Tcjt* **2004**, *4*, 41–71.
- (18) Hnát, J.; Paidar, M.; Bouzek, K.; Iulianelli, A.; Basile, A. *Current Trends and Future Developments on (Bio-) Membranes*; Elsevier: Amsterdam, 2020.
- (19) Hauch, A.; Ebbesen, S. D.; Jensen, S. H.; Mogensen, M. Highly efficient high temperature electrolysis. *J. Mater. Chem.* **2008**, *18*, 2331–2340.
- (20) Todd, D.; Schwager, M.; Mérida, W. Thermodynamics of high-temperature, high-pressure water electrolysis. *J. Power Sources* **2014**, *269*, 424–429.
- (21) Holm, T.; Borsboom-Hanson, T.; Herrera, O. E.; Mérida, W. Hydrogen costs from water electrolysis at high temperature and pressure. *Energy Convers. Manage.* **2021**, *237*, 114106.
- (22) Slowinski, E. J.; Gates, E. E.; Waring, C. E. The effect of pressure on the surface tensions of liquids. *J. Phys. Chem.* **1957**, *61*, 808–810.
- (23) Braun, L. Über die Absorption von Stickstoff und von Wasserstoff in wässrigen Lösungen verschieden dissociierter Stoffe. *Z. Phys. Chem.* **1900**, *33U*, 721–739.
- (24) Gertz, K.; Loeschcke, H. Bestimmung der Diffusions-Koeffizienten von H₂, O₂, N₂, und He in Wasser und Blutserum bei konstant gehaltener Konvektion. *Z. Naturforsch. B* **1954**, *9*, 1–9.
- (25) Chow, Y. T.; Maitland, G. C.; Trusler, J. P. Interfacial tensions of (H₂O + H₂) and (H₂O + CO₂ + H₂) systems at temperatures of (298–448) K and pressures up to 45 MPa. *Fluid Phase Equilib.* **2018**, *47S*, 37–44.
- (26) Massoudi, R.; King, A. D., Jr Effect of pressure on the surface tension of water. Adsorption of low molecular weight gases on water at 25 °C. *J. Phys. Chem.* **1974**, *78*, 2262–2266.
- (27) Hosseini, M.; Fahimpour, J.; Ali, M.; Keshavarz, A.; Iglauer, S. H₂-brine interfacial tension as a function of salinity, temperature, and pressure; implications for hydrogen geo-storage. *J. Pet. Sci. Eng.* **2022**, *213*, 110441.
- (28) Higgs, S.; Da Wang, Y.; Sun, C.; Ennis-King, J.; Jackson, S. J.; Armstrong, R. T.; Mostaghimi, P. In-situ hydrogen wettability characterisation for underground hydrogen storage. *Int. J. Hydrogen Energy* **2022**, *47*, 13062–13075.
- (29) Richards, T. W.; Carver, E. K. A critical study of the capillary rise method of determining surface tension, with data for water, benzene, toluene, chloroform, carbon tetrachloride, ether and dimethyl aniline.[second paper.]. *J. Am. Chem. Soc.* **1921**, *43*, 827–847.
- (30) Drelich, J.; Fang, C.; White, C. Measurement of interfacial tension in fluid-fluid systems. *Encycl. Surf. Colloid Sci.* **2002**, *3*, 3158–3163.
- (31) Chabab, S.; Théveneau, P.; Coquelet, C.; Corvisier, J.; Paricaud, P. Measurements and predictive models of high-pressure H₂ solubility in brine (H₂O+NaCl) for underground hydrogen storage application. *Int. J. Hydrogen Energy* **2020**, *45*, 32206–32220.
- (32) Torin-Ollarves, G. A.; Trusler, J. M. Solubility of hydrogen in sodium chloride brine at high pressures. *Fluid Phase Equilib.* **2021**, *539*, 113025.
- (33) Ansari, S.; Safaei-Farouji, M.; Atashrouz, S.; Abedi, A.; Hemmati-Sarapardeh, A.; Mohaddespour, A. Prediction of hydrogen solubility in aqueous solutions: Comparison of equations of state and advanced machine learning-metaheuristic approaches. *Int. J. Hydrogen Energy* **2022**, *47*, 37724.
- (34) Steiner, P. Ueber die Absorption des Wasserstoffs im Wasser und in wässrigen Lösungen. *Ann. Phys.* **1894**, *288*, 275–299.
- (35) Knopp, W. Über die Löslichkeitsbeeinflussung von Wasserstoff und Stickoxydul in wässrigen Lösungen verschieden dissoziierter Stoffe. *Z. Phys. Chem.* **1904**, *48U*, 97–108.
- (36) Gerecke, J.; Bittrich, H. The solubility of H₂, CO₂ and NH₃ in an aqueous electrolyte solution. *Wiss. Z. Tech. Hochsch. Chem. Carl Schorlemmer Leuna Merseburg* **1971**, *13*, 115–122.
- (37) Crozier, T. E.; Yamamoto, S. Solubility of Hydrogen in Water, Seawater, and NaCl Solutions. *J. Chem. Eng. Data* **1974**, *19*, 242–244.
- (38) Gordon, L. I.; Cohen, Y.; Standley, D. R. The solubility of molecular hydrogen in seawater. *Deep-Sea Res.* **1977**, *24*, 937–941.
- (39) Winkelmann, J. *Landolt-Bornstein: Numerical Data and Functional Relationships in Science and Technology, Group IV*, 1st ed.; Springer-Verlag: New York, 2007; Vol. 15A.
- (40) Baird, M. H. I.; Davidson, J. F. Annular jets-II: Gas absorption. *Chem. Eng. Sci.* **1962**, *17*, 473–480.
- (41) Houghton, G.; Wise, D. L. The diffusion coefficients of ten slightly soluble gases in water at 10–60° C. *Chem. Eng. Sci.* **1966**, *21*, 999–1010.
- (42) Akgerman, A.; Gainer, J. L. Predicting gas-liquid diffusivities. *J. Chem. Eng. Data* **1972**, *17*, 372–377.
- (43) Himmelblau, D. M. Diffusion of dissolved gases in liquids. *Chem. Rev.* **1964**, *64*, 527–550.
- (44) Verhallen, P. T. H. M.; Oomen, L. J. P.; Elsen, A. J. J. M.; Kruger, J.; Fortuin, J. M. H. The diffusion coefficients of helium, hydrogen, oxygen and nitrogen in water determined from the permeability of a stagnant liquid layer in the quasi-s. *Chem. Eng. Sci.* **1984**, *39*, 1535–1541.
- (45) Jähne, B.; Heinz, G.; Dietrich, W. Measurement of the diffusion coefficients of sparingly soluble gases in water. *J. Geophys. Res.: Oceans* **1987**, *92*, 10767–10776.
- (46) De Blok, W. J.; Fortuin, J. M. H. Method for determining diffusion coefficients of slightly soluble gases in liquids. *Chem. Eng. Sci.* **1981**, *36*, 1687–1694.
- (47) Nielsen, L. C.; Bourg, I. C.; Sposito, G. Predicting CO₂-water interfacial tension under pressure and temperature conditions of geologic CO₂ storage. *Geochim. Cosmochim. Acta* **2012**, *81*, 28–38.
- (48) Li, X.; Ross, D. A.; Trusler, J. P. M.; Maitland, G. C.; Boek, E. S. Molecular dynamics simulations of CO₂ and brine interfacial tension at high temperatures and pressures. *J. Phys. Chem. B* **2013**, *117*, 5647–5652.
- (49) Liu, Y.; Lafitte, T.; Panagiotopoulos, A. Z.; Debenedetti, P. G. Simulations of vapor-liquid phase equilibrium and interfacial tension in the CO₂-H₂O-NaCl system. *AIChE J.* **2013**, *59*, 3514–3522.

- (50) Tsuji, S.; Liang, Y.; Kunieda, M.; Takahashi, S.; Matsuoka, T. Molecular Dynamics Simulations of the CO₂-Water-silica Interfacial Systems. *Energy Procedia* **2013**, *37*, 5435–5442.
- (51) Knauer, S.; Schenk, M. R.; Koddermann, T.; Reith, D.; Jaeger, P. Interfacial tension and related properties of ionic liquids in CH₄ and CO₂ at elevated pressures: experimental data and molecular dynamics simulation. *J. Chem. Eng. Data* **2017**, *62*, 2234–2243.
- (52) Hosseinzadeh Dehaghani, Y.; Assareh, M.; Feyzi, F. Simultaneous Prediction of Equilibrium, Interfacial, and Transport Properties of CO₂-Brine Systems Using Molecular Dynamics Simulation: Applications to CO₂ Storage. *Ind. Eng. Chem. Res.* **2022**, *61*, 15390–15406.
- (53) Zhao, L.; Ji, J.; Tao, L.; Lin, S. Ionic effects on supercritical CO₂-brine interfacial tensions: Molecular dynamics simulations and a universal correlation with ionic strength, temperature, and pressure. *Langmuir* **2016**, *32*, 9188–9196.
- (54) Yang, Y.; Narayanan Nair, A. K.; Sun, S. Molecular dynamics simulation study of carbon dioxide, methane, and their mixture in the presence of brine. *J. Phys. Chem. B* **2017**, *121*, 9688–9698.
- (55) Papavasileiou, K. D.; Moults, O. A.; Economou, I. G. Predictions of water/oil interfacial tension at elevated temperatures and pressures: A molecular dynamics simulation study with biomolecular force fields. *Fluid Phase Equilib.* **2018**, *476*, 30–38.
- (56) Aminian, A.; ZareNezhad, B. Molecular dynamics simulations study on the shear viscosity, density, and equilibrium interfacial tensions of CO₂ + brines and brines + CO₂ + n-decane systems. *J. Phys. Chem. B* **2021**, *125*, 2707–2718.
- (57) Blazquez, S.; Zeron, I.; Conde, M.; Abascal, J.; Vega, C. Scaled charges at work: Salting out and interfacial tension of methane with electrolyte solutions from computer simulations. *Fluid Phase Equilib.* **2020**, *513*, 112548.
- (58) Kallikragas, D. T.; Plugatyr, A. Y.; Svishev, I. M. High temperature diffusion coefficients for O₂, H₂, and OH in water, and for pure water. *J. Chem. Eng. Data* **2014**, *59*, 1964–1969.
- (59) Zhao, X.; Jin, H. Investigation of hydrogen diffusion in supercritical water: A molecular dynamics simulation study. *Int. J. Heat Mass Transfer* **2019**, *133*, 718–728.
- (60) Tsimpanogiannis, I. N.; Maity, S.; Celebi, A. T.; Moults, O. A. Engineering Model for Predicting the Intradiffusion Coefficients of Hydrogen and Oxygen in Vapor, Liquid, and Supercritical Water based on Molecular Dynamics Simulations. *J. Chem. Eng. Data* **2021**, *66*, 3244.
- (61) Zhao, X.; Jin, H. Correlation for self-diffusion coefficients of H₂, CH₄, CO, O₂ and CO₂ in supercritical water from molecular dynamics simulation. *Appl. Therm. Eng.* **2020**, *171*, 114941.
- (62) Zhao, X.; Jin, H.; Chen, Y.; Ge, Z. Numerical study of H₂, CH₄, CO, O₂ and CO₂ diffusion in water near the critical point with molecular dynamics simulation. *Comput. Math. with Appl.* **2021**, *81*, 759–771.
- (63) Marx, D.; Nielaba, P. Path-integral Monte Carlo techniques for rotational motion in two dimensions: Quenched, annealed, and no-spin quantum-statistical averages. *Phys. Rev. A* **1992**, *45*, 8968.
- (64) Köster, A.; Thol, M.; Vrabec, J. Molecular Models for the Hydrogen Age: Hydrogen, Nitrogen, Oxygen, Argon, and Water. *J. Chem. Eng. Data* **2018**, *63*, 305–320.
- (65) Buch, V. Path integral simulations of mixed para-D₂ and ortho-D-2 clusters: The orientational effects. *J. Chem. Phys.* **1994**, *100*, 7610–7629.
- (66) Hirschfelder, J. O.; Curtiss, C. F.; Bird, R. B. *Molecular theory of gases and liquids*, 1st ed.; John Wiley: New York, 1964.
- (67) Cracknell, R. F. Molecular Simulation of hydrogen adsorption in graphitic nanofibres. *Phys. Chem. Chem. Phys.* **2001**, *3*, 2091–2097.
- (68) Alavi, S.; Ripmeester, J.; Klug, D. Molecular-dynamics study of structure II hydrogen clathrates. *J. Chem. Phys.* **2005**, *123*, 024507.
- (69) Abascal, J. L.; Vega, C. A general purpose model for the condensed phases of water: TIP4P/2005. *J. Chem. Phys.* **2005**, *123*, 234505.
- (70) Garcia-Ratés, M.; de Hemptinne, J.-C.; Avalos, J. B.; Nieto-Draghi, C. Molecular Modeling of Diffusion Coefficient and Ionic Conductivity of CO₂ in Aqueous Ionic Solutions. *J. Phys. Chem. B* **2012**, *116*, 2787–2800.
- (71) Aimoli, C. G.; Maginn, E. J.; Abreu, C. R. Transport properties of carbon dioxide and methane from molecular dynamics simulations. *J. Chem. Phys.* **2014**, *141*, 134101.
- (72) Zhong, H.; Lai, S.; Wang, J.; Qiu, W.; Ludemann, H.-D.; Chen, L. Molecular dynamics simulation of transport and structural properties of CO₂ using different molecular models. *J. Chem. Eng. Data* **2015**, *60*, 2188–2196.
- (73) Jiang, H.; Economou, I. G.; Panagiotopoulos, A. Z. Molecular modeling of thermodynamic and transport properties for CO₂ and aqueous brines. *Acc. Chem. Res.* **2017**, *50*, 751–758.
- (74) Lopez-Lazaro, C.; Bachaud, P.; Moretti, I.; Ferrando, N. Predicting the phase behavior of hydrogen in NaCl brines by Molecular Simulation for geological applications. *BSGF-Earth Sci. Bulletin* **2019**, *190*, 7.
- (75) Liu, Y.; Panagiotopoulos, A. Z.; Debenedetti, P. G. Monte Carlo simulations of high-pressure phase equilibria of CO₂-H₂O mixtures. *J. Phys. Chem. B* **2011**, *115*, 6629–6635.
- (76) Liu, Y.; Lafitte, T.; Panagiotopoulos, A. Z.; Debenedetti, P. G. Simulations of vapor-liquid phase equilibrium and interfacial tension in the CO₂-H₂O-NaCl system. *AIChE J.* **2013**, *59*, 3514–3522.
- (77) Habibi, P.; Rahbari, A.; Blazquez, S.; Vega, C.; Dey, P.; Vlucht, T. J. H.; Moults, O. A. A New Force Field for OH- for Computing Thermodynamic and Transport Properties of H₂ and O₂ in Aqueous NaOH and KOH Solutions. *J. Phys. Chem. B* **2022**, *126*, 9376–9387.
- (78) Rahbari, A.; Hens, R.; Ramdin, M.; Moults, O. A.; Dubbeldam, D.; Vlucht, T. J. H. Recent advances in the Continuous Fractional Component Monte Carlo methodology. *Mol. Simul.* **2021**, *47*, 804–823.
- (79) Shi, W.; Maginn, E. J. Continuous Fractional Component Monte Carlo: an adaptive biasing method for open system atomistic simulations. *J. Chem. Theory Comput.* **2007**, *3*, 1451–1463.
- (80) Shi, W.; Maginn, E. J. Improvement in molecule exchange efficiency in Gibbs ensemble Monte Carlo: Development and implementation of the Continuous Fractional Component move. *J. Comput. Chem.* **2008**, *29*, 2520–2530.
- (81) Zeron, I. M.; Abascal, J. L. F.; Vega, C. A force field of Li⁺, Na⁺, K⁺, Mg²⁺, Ca²⁺, Cl⁻, and SO₄²⁻ in aqueous solution based on the TIP4P/2005 water model and scaled charges for the ions. *J. Chem. Phys.* **2019**, *151*, 104501.
- (82) Blazquez, S.; Conde, M. M.; Vega, C. Unpublished. 2023.
- (83) Vega, C.; Abascal, J. L. Simulating water with rigid non-polarizable models: a general perspective. *Phys. Chem. Chem. Phys.* **2011**, *13*, 19663–19688.
- (84) Tsimpanogiannis, I. N.; Moults, O. A.; Franco, L. F.; Spera, M. B. M.; Erdős, M.; Economou, I. G. Self-diffusion coefficient of bulk and confined water: a critical review of classical Molecular Simulation studies. *Mol. Simul.* **2019**, *45*, 425–453.
- (85) González, M. A.; Abascal, J. L. The shear viscosity of rigid water models. *J. Chem. Phys.* **2010**, *132*, 096101.
- (86) Moults, O. A.; Tsimpanogiannis, I. N.; Panagiotopoulos, A. Z.; Economou, I. G. Atomistic molecular dynamics simulations of CO₂ diffusivity in H₂O for a wide range of temperatures and pressures. *J. Phys. Chem. B* **2014**, *118*, 5532–5541.
- (87) Sakamaki, R.; Sum, A. K.; Narumi, T.; Ohmura, R.; Yasuoka, K. Thermodynamic properties of methane/water interface predicted by molecular dynamics simulations. *J. Chem. Phys.* **2011**, *134*, 144702.
- (88) Vega, C.; de Miguel, E. Surface tension of the most popular models of water by using the test-area simulation method. *J. Chem. Phys.* **2007**, *126*, 154707.
- (89) Döpke, M. F.; Moults, O. A.; Hartkamp, R. On the transferability of ion parameters to the TIP4P/2005 water model using molecular dynamics simulations. *J. Chem. Phys.* **2020**, *152*, 024501.
- (90) Deeg, K. S.; Gutiérrez-Sevillano, J. J.; Bueno-Pérez, R.; Parra, J. B.; Ania, C. O.; Doblaré, M.; Calero, S. Insights on the Molecular Mechanisms of Hydrogen Adsorption in Zeolites. *J. Phys. Chem. C* **2013**, *117*, 14374–14380.

- (91) Sesé, L. M. Study of the Feynman-Hibbs effective potential against the path-integral formalism for Monte Carlo simulations of quantum many-body Lennard-Jones systems. *Mol. Phys.* **1994**, *81*, 1297–1312.
- (92) Sesé, L. M. Feynman-Hibbs potentials and path integrals for quantum Lennard-Jones systems: Theory and Monte Carlo simulations. *Mol. Phys.* **1995**, *85*, 931–947.
- (93) Rahbari, A.; Brenkman, J.; Hens, R.; Ramdin, M.; van den Broeke, L. J. P.; Schoon, R.; Henkes, R.; Moulto, O. A.; Vlught, T. J. H. Solubility of water in hydrogen at high pressures: A Molecular Simulation study. *J. Chem. Eng. Data* **2019**, *64*, 4103–4115.
- (94) Plimpton, S. Fast Parallel Algorithms for Short-Range Molecular Dynamics. *J. Comput. Phys.* **1995**, *117*, 1–19.
- (95) Ryckaert, J. P.; Ciccotti, G.; Berendsen, H. J. Numerical integration of the cartesian equations of motion of a system with constraints: molecular dynamics of n-alkanes. *J. Comput. Phys.* **1977**, *23*, 327–341.
- (96) Allen, M. P.; Tildesley, D. J. *Computer simulation of liquids*; Oxford University Press, 2017.
- (97) Frenkel, D.; Smit, B. *Understanding Molecular Simulation: from algorithms to applications*, 2nd ed.; Elsevier: San Diego, 2002.
- (98) Hockney, R.; Eastwood, J. *Computer Simulation Using Particles*, 1st ed.; CRC Press: New York, 1988.
- (99) Plimpton, S. *LAMMPS Documentation (15 Sep 2022 version)*. <https://docs.lammps.org/Manual.html> (accessed: 26/10/2022).
- (100) Martínez, L.; Andrade, R.; Birgin, E. G.; Martínez, J. M. PACKMOL: A package for building initial configurations for molecular dynamics simulations. *J. Comput. Chem.* **2009**, *30*, 2157–2164.
- (101) Isele-Holder, R. E.; Mitchell, W.; Ismail, A. E. Development and application of a particle-particle particle-mesh Ewald method for dispersion interactions. *J. Chem. Phys.* **2012**, *137*, 174107.
- (102) Salehi, H. S.; Moulto, O. A.; Vlught, T. J. H. Interfacial Properties of Hydrophobic Deep Eutectic Solvents with Water. *J. Phys. Chem. B* **2021**, *125*, 12303–12314.
- (103) Rowlinson, J. S.; Widom, B. *Molecular theory of capillarity*, 1st ed.; Courier Corporation: Oxford, 1982.
- (104) Jamali, S. H.; Wolff, L.; Becker, T. M.; de Groen, M.; Ramdin, M.; Hartkamp, R.; Bardow, A.; Vlught, T. J. H.; Moulto, O. A. OCTP: A Tool for On-the-Fly Calculation of Transport Properties of Fluids with the Order- n Algorithm in LAMMPS. *J. Chem. Inf. Model.* **2019**, *59*, 1290–1294.
- (105) Dubbeldam, D.; Ford, D. C.; Ellis, D. E.; Snurr, R. Q. A new perspective on the order- n algorithm for computing correlation functions. *Mol. Simul.* **2009**, *35*, 1084–1097.
- (106) Yeh, I.-C.; Hummer, G. System-size dependence of diffusion coefficients and viscosities from molecular dynamics simulations with periodic boundary conditions. *J. Phys. Chem. B* **2004**, *108*, 15873–15879.
- (107) Celebi, A. T.; Jamali, S. H.; Bardow, A.; Vlught, T. J. H.; Moulto, O. A. Finite-size effects of diffusion coefficients computed from molecular dynamics: a review of what we have learned so far. *Mol. Simul.* **2021**, *47*, 831–845.
- (108) Jamali, S. H.; Bardow, A.; Vlught, T. J. H.; Moulto, O. A. Generalized form for finite-size corrections in mutual diffusion coefficients of multicomponent mixtures obtained from equilibrium molecular dynamics simulation. *J. Chem. Theory Comput.* **2020**, *16*, 3799–3806.
- (109) Moulto, O. A.; Zhang, Y.; Tsimpanogiannis, I. N.; Economou, I. G.; Maginn, E. J. System-size corrections for self-diffusion coefficients calculated from molecular dynamics simulations: The case of CO₂, n-alkanes, and poly (ethylene glycol) dimethyl ethers. *J. Chem. Phys.* **2016**, *145*, 074109.
- (110) Jamali, S. H.; Hartkamp, R.; Bardas, C.; Sohl, J.; Vlught, T. J. H.; Moulto, O. A. Shear viscosity computed from the finite-size effects of self-diffusivity in equilibrium molecular dynamics. *J. Chem. Theory Comput.* **2018**, *14*, 5959–5968.
- (111) Jamali, S. H.; Wolff, L.; Becker, T. M.; Bardow, A.; Vlught, T. J. H.; Moulto, O. A. Finite-size effects of binary mutual diffusion coefficients from molecular dynamics. *J. Chem. Theory Comput.* **2018**, *14*, 2667–2677.
- (112) Hens, R.; Rahbari, A.; Caro-Ortiz, S.; Dawass, N.; Erdos, M.; Poursaeidesfahani, A.; Salehi, H. S.; Celebi, A. T.; Ramdin, M.; Moulto, O. A.; Dubbeldam, D.; Vlught, T. J. H. Brick-CFCMC: Open Source Software for Monte Carlo Simulations of Phase and Reaction Equilibria Using the Continuous Fractional Component Method. *J. Chem. Inf. Model.* **2020**, *60*, 2678–2682.
- (113) Polat, H. M.; Salehi, H. S.; Hens, R.; Wasik, D. O.; Rahbari, A.; de Meyer, F.; Houriez, C.; Coquelet, C.; Calero, S.; Dubbeldam, D.; Moulto, O. A.; Vlught, T. J. H. New Features of the Open Source Monte Carlo Software Brick-CFCMC: Thermodynamic Integration and Hybrid Trial Moves. *J. Chem. Inf. Model.* **2021**, *61*, 3752–3757.
- (114) Poursaeidesfahani, A.; Hens, R.; Rahbari, A.; Ramdin, M.; Dubbeldam, D.; Vlught, T. J. H. Efficient application of Continuous Fractional Component Monte Carlo in the reaction ensemble. *J. Chem. Theory Comput.* **2017**, *13*, 4452–4466.
- (115) Rahbari, A.; Hens, R.; Dubbeldam, D.; Vlught, T. J. H. Improving the accuracy of computing chemical potentials in CFCMC simulations. *Mol. Phys.* **2019**, *117*, 3493–3508.
- (116) Rahbari, A.; Hens, R.; Jamali, S.; Ramdin, M.; Dubbeldam, D.; Vlught, T. J. H. Effect of truncating electrostatic interactions on predicting thermodynamic properties of water-methanol systems. *Mol. Simul.* **2019**, *45*, 336–350.
- (117) Wang, F.; Landau, D. P. Efficient multiple-range random walk algorithm to calculate the density of states. *Phys. Rev. Lett.* **2001**, *86*, 2050.
- (118) Wang, F.; Landau, D. P. Determining the density of states for classical statistical models: A random walk algorithm to produce a flat histogram. *Phys. Rev. E* **2001**, *64*, 056101.
- (119) Salehi, H. S.; Hens, R.; Moulto, O. A.; Vlught, T. J. H. Computation of gas solubilities in choline chloride urea and choline chloride ethylene glycol deep eutectic solvents using Monte Carlo simulations. *J. Mol. Liq.* **2020**, *316*, 113729.
- (120) Widom, B. Potential-distribution theory and the statistical mechanics of fluids. *J. Phys. Chem.* **1982**, *86*, 869–872.
- (121) Widom, B. Some Topics in the Theory of Fluids. *J. Chem. Phys.* **1963**, *39*, 2808–2812.
- (122) Rahbari, A.; Hens, R.; Nikolaidis, I. K.; Poursaeidesfahani, A.; Ramdin, M.; Economou, I. G.; Moulto, O. A.; Dubbeldam, D.; Vlught, T. J. H. Computation of partial molar properties using continuous fractional component Monte Carlo. *Mol. Phys.* **2018**, *116*, 3331–3344.
- (123) Georgiadis, A.; Maitland, G.; Trusler, J. M.; Bismarck, A. Interfacial tension measurements of the (H₂O+ CO₂) system at elevated pressures and temperatures. *J. Chem. Eng. Data* **2010**, *55*, 4168–4175.
- (124) Bachu, S.; Bennion, D. B. Interfacial tension between CO₂, freshwater, and brine in the range of pressure from (2 to 27) MPa, temperature from (20 to 125) °C, and water salinity from (0 to 334 000) mg·L⁻¹. *J. Chem. Eng. Data* **2009**, *54*, 765–775.
- (125) Hebach, A.; Oberhof, A.; Dahmen, N.; Kögel, A.; Ederer, H.; Dinjus, E. Interfacial tension at elevated pressures measurements and correlations in the water+ carbon dioxide system. *J. Chem. Eng. Data* **2002**, *47*, 1540–1546.
- (126) Ren, Q.-Y.; Chen, G.-J.; Yan, W.; Guo, T.-M. Interfacial tension of (CO₂+ CH₄)₂+ water from 298 to 373 K and pressures up to 30 MPa. *J. Chem. Eng. Data* **2000**, *45*, 610–612.
- (127) Naeiji, P.; Woo, T. K.; Alavi, S.; Ohmura, R. Molecular dynamics simulations of interfacial properties of the CO₂-water and CO₂-CH₄-water systems. *J. Chem. Phys.* **2020**, *153*, 044701.
- (128) Li, X.; Boek, E.; Maitland, G. C.; Trusler, J. P. M. Interfacial Tension of (Brines+ CO₂):(0.864 NaCl+ 0.136 KCl) at Temperatures between (298 and 448) K, Pressures between (2 and 50) MPa, and Total Molalities of (1 to 5) mol·kg⁻¹. *J. Chem. Eng. Data* **2012**, *57*, 1078–1088.
- (129) Aggelopoulos, C. A.; Robin, M.; Vizika, O. Interfacial tension between CO₂ and brine (NaCl+ CaCl₂) at elevated pressures and

temperatures: The additive effect of different salts. *Adv. Water Resour.* **2011**, *34*, 505–511.

(130) Jerauld, G. R.; Kazemi, A. An improved simple correlation for accurate estimation of CO₂-Brine interfacial tension at reservoir conditions. *J. Pet. Sci. Eng.* **2022**, *208*, 109537.

(131) Manciu, M.; Ruckenstein, E. Specific ion effects via ion hydration: I. Surface tension. *Adv. Colloid Interface Sci.* **2003**, *105*, 63–101.

(132) Marcus, Y. Effect of ions on the structure of water: Structure making and breaking. *Chem. Rev.* **2009**, *109*, 1346–1370.

(133) Pegram, L. M.; Record, M. T. Hofmeister salt effects on surface tension arise from partitioning of anions and cations between bulk water and the air-water interface. *J. Phys. Chem. B* **2007**, *111*, 5411–5417.

(134) Levin, Y.; dos Santos, A. P.; Diehl, A. Ions at the air-water interface: An end to a hundred-year-old mystery? *Phys. Rev. Lett.* **2009**, *103*, 257802.

(135) Weisenberger, S.; Schumpe, A. Estimation of gas solubilities in salt solutions at temperatures from 273 to 363 K. *AIChE J.* **1996**, *42*, 298–300.

(136) Laliberté, M. Model for calculating the viscosity of aqueous solutions. *J. Chem. Eng. Data* **2007**, *52*, 321–335.

(137) Laliberté, M.; Cooper, W. E. Model for calculating the density of aqueous electrolyte solutions. *J. Chem. Eng. Data* **2004**, *49*, 1141–1151.

(138) Tsimpanogiannis, I. N.; Moulton, O. A. Is Stokes-Einstein relation valid for the description of intra-diffusivity of hydrogen and oxygen in liquid water? *Fluid Phase Equilib.* **2022**, *563*, 113568.

(139) Cussler, E. L. *Diffusion Coefficients and Diffusion of Interacting Species*, 2nd ed.; Cambridge University Press: Cambridge, 2009.

(140) Taylor, R.; Krishna, R. *Multicomponent mass transfer*, 1st ed.; John Wiley & Sons, 1993; Vol. 2.

(141) Krishna, R.; Wesselingh, J. The Maxwell-Stefan approach to mass transfer. *Chem. Eng. Sci.* **1997**, *52*, 861–911.

(142) Wiebe, R.; Gaddy, V. L. The Solubility of Hydrogen in Water at 0, 50, 75 and 100° from 25 to 1000 atm. *J. Am. Chem. Soc.* **1934**, *56*, 76–79.

(143) Wiebe, R.; Gaddy, V.; Heins, C. Solubility of Hydrogen in Water at 25° C. from 25 to 1000 atm. *Ind. Eng. Chem.* **1932**, *24*, 823–825.

(144) Kling, G.; Maurer, G. The solubility of hydrogen in water and in 2-aminoethanol at temperatures between 323 and 423 K and pressures up to 16 MPa. *J. Chem. Thermodyn.* **1991**, *23*, 531–541.

(145) Choudhary, V. R.; Parande, M. G.; Brahme, P. H. Simple apparatus for measuring solubility of gases at high pressures. *Ind. Eng. Chem. Fundam.* **1982**, *21*, 472–474.

(146) Chandrasekhar, J.; Spellmeyer, D. C.; Jorgensen, W. L. Energy component analysis for dilute aqueous solutions of lithium (1+), sodium (1+), fluoride (1-), and chloride (1-) ions. *J. Am. Chem. Soc.* **1984**, *106*, 903–910.

(147) Darkrim, F.; Vermesse, J.; Malbrunot, P.; Levesque, D. Monte Carlo simulations of nitrogen and hydrogen physisorption at high pressures and room temperature. Comparison with experiments. *J. Chem. Phys.* **1999**, *110*, 4020–4027.

(148) Zhu, Z.; Cao, Y.; Zheng, Z.; Chen, D. An Accurate Model for Estimating H₂ Solubility in Pure Water and Aqueous NaCl Solutions. *Energies* **2022**, *15*, 5021.

Recommended by ACS

Density and Volumetric Behavior of Ternary CO₂ + *n*-Decane + *n*-Butylcyclohexane Mixtures at High Pressure and High Temperature

Angélica María Chacón Valero, Hosiberto Batista de Sant'Ana, *et al.*

MAY 25, 2022

JOURNAL OF CHEMICAL & ENGINEERING DATA

READ 

Henry's Law Constants and Vapor-Liquid Distribution Coefficients of Noncondensable Gases Dissolved in Carbon Dioxide

Sergey B. Martynov, Haroun Mahgerefteh, *et al.*

MARCH 02, 2022

ACS OMEGA

READ 

Molecular Simulation Study on the Density Behavior of *n*-Alkane/CO₂ Systems

Youhui Wang, Jun Liu, *et al.*

OCTOBER 29, 2021

ACS OMEGA

READ 

Transferable Anisotropic United-Atom Mie (TAMie) Force Field: Transport Properties from Equilibrium Molecular Dynamic Simulations

Matthias Fischer, Joachim Gross, *et al.*

APRIL 13, 2020

INDUSTRIAL & ENGINEERING CHEMISTRY RESEARCH

READ 

Get More Suggestions >